HHS Public Access

Author manuscript

Dev Biol. Author manuscript; available in PMC 2018 October 01.

Published in final edited form as:

Dev Biol. 2017 October 01; 430(1): 11–17. doi:10.1016/j.ydbio.2017.07.017.

A defect in the mitochondrial protein *mpv17* underlies the transparent *casper* zebrafish

Gianluca D'Agati[1], **Rosanna Beltre**[2], **Anna Sessa**[2], **Alexa Burger**[1], **Yi Zhou**[2], **Christian Mosimann**[1], and **Richard M. White**[3,4]

[1]Institute of Molecular Life Sciences, University of Zürich, Zürich, Switzerland [2]Hematology & Oncology, Children's Hospital Boston, Boston MA [3]Cancer Biology & Genetics, Memorial Sloan Kettering Cancer Center, New York, NY [4]Department of Medicine, Memorial Sloan Kettering Cancer Center, New York, NY

Abstract

The *casper* strain of zebrafish is widely used in studies ranging from cancer to neuroscience. *casper* offers the advantage of relative transparency throughout adulthood, making it particularly useful for *in vivo* imaging by epifluorescence, confocal, and light sheet microscopy. *casper* was developed by selective breeding of two previously described recessive pigment mutants: 1) *nacre*, which harbors an inactivating mutation of the *mitfa* gene, rendering the fish devoid of pigmented melanocytes; and 2) *roy orbison*, a mutant with so-far unidentified genetic cause that lacks reflective iridophores. To clarify the molecular nature of the *roy orbison* mutation, such that it can inform studies using *casper,* we undertook an effort to positionally clone the *roy orbison* mutation. We find that *roy orbison* is caused by an intronic defect in the gene *mpv17*, encoding an inner mitochondrial membrane protein that has been implicated in human mitochondrial DNA depletion syndrome. The *roy orbison* mutation is phenotypically and molecularly remarkably similar to another zebrafish iridophore mutant called *transparent.* Using Cas9-induced crispants and germline mutants with disrupted *mpv17* open reading frame, we show in trans-heterozygote embryos that new frameshift alleles of *mpv17*, *roy orbison*, and *transparent* fail to complement each other. Our work provides genetic evidence that both *roy orbison* and *transparent* affect the *mpv17* locus by a similar if not identical genetic lesion. Identification of *mpv17* mutants will allow for further work probing the relationship between mitochondrial function and pigmentation, which has to date received little attention.

INTRODUCTION

The three classes of zebrafish pigment cells - melanophores, xanthophores and iridophores - combine to give the adult fish its characteristic pigmentation pattern (McGowan and Barsh,

Correspondence to: Christian Mosimann; Richard M. White.

2016; Parichy and Spiewak, 2015; Rawls et al., 2001). Mutants with defects in one or more of these cells have yielded important insights into the genes regulating vertebrate pigmentation. For example, the zebrafish *nacre* (*nac*) mutant harbors an an inactivating mutation in the *mitfa* gene and are devoid of nearly all embryonic and adult melanophores (Lister et al., 1999), emphasizing the key role of this transcription factor as a master regulator of this cell type. Mutants with defects in iridophores are somewhat less common, but several have been observed including *ltk*/*shady* (*shd*) (Lopes et al., 2008), *ednrba* (*rose*) (Parichy et al., 2000), *transparent* (*tra*) (Krauss et al., 2013), and *roy orbison* (*roy*) (Ren et al., 2002).

Combinations of these pigmentation mutants have been used to yield adult zebrafish that are more transparent than the typical adult. Combining the *mitfa* allele nac^{w2} with the *roy* mutant yielded the *casper* strain (White et al., 2008); since *casper* lacks all light-absorbing melanophores as well as all light-reflecting iridophores, the strain is optimal for imaging of deeper structures throughout the life-cycle of the fish. The *casper* strain has been broadly applied to numerous imaging applications in the zebrafish field; however, a remaining caveat remains that the affected gene responsible for the *roy orbison* phenotype has remained unknown. To address this, we aimed to positionally clone and validate the causative mutation. Here, we provide sequencing and genetic evidence that the phenotype of *roy* is due to a defect in the mitochondrial inner membrane protein *mpv17*, which has previously been associated with the mitochondrial DNA depletion syndrome in mammals (Löllgen and Weiher, 2015). Our data reveals that the *roy* allele causes aberrant splicing due to a perturbation in the first intron of *mpv17*. Importantly, a recent publication linked the highly similar mutant *tra* to the identical defect in the *mpv17* mRNA (Krauss et al., 2013), suggesting these two mutants are caused by similar or even the same lesion. By genetic complementation analysis with Cas9-induced *de novo* loss-of-function alleles that directly disrupt the open reading frame (ORF) of *mpv17*, we confirm that both *roy* and *tra* are allelic to *mpv17* and to each other. Our work underlines the value of newly generated mutant alleles to resolve the causation of genetic lesions. Little information is available connecting mitochondrial function in pigmentation lineages and iridophores specifically, but will be an important future area of investigation for the field of vertebrate pigmentation.

RESULTS

roy orbison contributes to casper by iridophore loss and secondary effects on pigmentation

The most obvious phenotype of the recessive *roy* mutant is a severe, near complete loss of reflective iridophores in both embryos and adults (Figure 1). This gives the eyes its characteristic black appearance (vaguely resembling the popular image of the singer of the same name), in contrast to a wildtype (*AB*) fish in which the eyes are covered with iridophores. Although embryonic melanocyte development appears largely normal, we noted a severe defect in adult melanocyte formation in *roy*, which is likely due to the loss of nearby iridophores. We did not observe a strong defect in xanthophores, the other major pigment class found in the zebrafish. The major additional defect in *casper* is a loss of all

pigmented melanocytes due to the mutation in the *mitfa* gene caused by the *nacre* allele, as previously described (White et al., 2008), (Lister et al., 1999).

Positional cloning of roy orbison

The *roy* mutant is homozygous viable. We outcrossed adult mutants to the WIK strain of zebrafish to perform low-level genome mapping as previously described (Zhou and Zon, 2011). This revealed the localization of the *roy* mutation on zebrafish linkage group 20 (Figure 2A). We then used a panel of well-validated SNP markers to narrow down the likely chromosomal location, and found that the *roy* mutation was located between markers *z13672* (75.7cM) and *z28453* (91.0cM). We refined this position using further SNP markers *zp10* and *zp61* that resulted in 4/792 and 5/1496 recombinants, respectively.

By examining the candidate region in the UCSC browser, we noted only 8 genes in the region flanked by these markers: *scdr9, dnj14, trim54, uts1, mpv17, uckl1, slc20a2.* We performed quantitative RT-PCR on whole embryos for each of these 8 genes to narrow down the putative candidates, reasoning that a mutation could lead to nonsense-mediated decay (NMD) of the mRNA (Figure 2B). We detected a clear downregulation of *dnj14* and *mpv17*. Given the identification of *mpv17* as affected gene in the *transparent* mutant (tra^{b6}, also referred to as tra^{b18}) (Krauss et al., 2013) and given the striking recessive pigmentation phenotype of *roy*, we reasoned that *mpv17* was the likely causative gene for the *roy orbison* phenotype.

roy orbison features a 19bp deletion in the mpv17 mRNA

We isolated and reverse-transcribed mRNA from *AB* wildtypes and *roy* mutants before sequencing multiple cDNA clones to detect potential mutations in *mpv17*. In all 3 *roy* clones, we identified a 19 bp deletion that results in aberrant splicing between the exons 2 and 3 of *mpv17* (Figure 2C). This leads to a frameshift and early stop codon that likely yields a null for the protein. To identify the cause of the splicing defect, we sequenced genomic DNA corresponding to exons 2 and 3 from AB and mutant fish, but could not detect any exonic mutations that would have caused the splicing defect. We therefore assumed that the underlying genomic defect occurs in the intron between exons 2 and 3, but we repeatedly failed to amplify the genomic DNA from intron 2–3, suggesting there is a deletion in this intron that leads to aberrant splicing and subsequent early stop of the mRNA. Our findings are remarkably similar to the recent reports of cloning the spontaneous tra^{b6} mutant by Krauss et al. (Krauss et al., 2013), who found the identical splice defect and issues with amplifying intron 2–3 in their study.

mpv17 mRNA rescues the roy orbison phenotype

Given that intron 2–3 spans approximately 20kb and we repeatedly failed at isolating any PCR products, we instead decided to functionally test whether *mpv17* was the causative gene underlying the *roy* phenotype. We isolated the full-length *mpv17* ORF from the AB strain as above, cloned it into *pCS2+*, and then used this vector to *in vitro*-synthesize capped, polyadenylated *mpv17* mRNA. We injected the *mpv17* mRNA into the yolk of single-cell stage embryos from a homozygous *roy* incross at a concentration of 100 ng/μl. Of the 20 fish that survived to 4 dpf, 16/20 had fully rescued eye iridophores (Figure 3A). We also injected

the mRNA into WT AB strain fish and did not observe any obvious phenotypes. These observations suggest that supplementing homozygous *roy* embryos with functional *mpv17*-encoding mRNA rescues the mutant phenotype.

Morpholino knockdown of mpv17

We next injected an ATG morpholino against *mpv17* into wildtype embryos derived from an incross of the *AB* strain (Figure 3B,C). We examined the injected embryos at 4–7 dpf and noted a range of phenotypes, with 87% of embryos showing either complete (72%, n=48/67) or moderate (16%, n=11/67) loss of iridophores. Only 12% of the injected fish had normal appearing iridophores, in contrast to 89% of the uninjected AB embryos ($p<0.05$, uninjected vs. injected embryos, paired t-test). Although the majority of the remaining embryos were phenotypically normal, we did note some animals with defects in heart development, which may represent a nonspecific toxicity of the morpholino since we did not observe a similar phenotype in *roy* mutants.

Cas9-mediated mutagenesis of the mpv17 ORF reproduces the roy orbison phenotype

To genetically confirm the mapped mutation and to generate *de novo* alleles of *mpv17* that directly perturb the ORF, we sought to target *mpv17* using CRISPR-Cas9 (Figure 4A). We injected wildtype embryos with solubilized, fluorescent Cas9-sgRNA ribonucleoprotein complexes (RNPs) using sgRNAs to target the *mpv17* ORF either in exon 2 (sgRNA *ccB*) or in exon 3 (sgRNA *ccC*). Both sgRNAs caused comparable effects. Embryos injected with the $mpv17^{ccB}$ sgRNA displayed a specific, strong reduction of iridophores predominantly in the eye and trunk region (Figure 4B,C); an average of 77% (n=172/223) of CRISPR-injected F0 embryos (so-called crispants) consistently featured iridophore loss (Figure 4D). *mpv17* crispants showed no apparent other phenotype than iridophore loss and did not have a significantly higher mortality than uninjected siblings at 5 dpf. Sanger sequencing from PCR-isolated clones of the sgRNA target region in injected individuals and allele-level analysis with CrispRVariants (Burger et al., 2016; Lindsay et al., 2016) revealed exceedingly high mutagenesis efficiency, with frameshift deletions as most predominant mutation event that is predicted to result in early termination of translation (Supplemental Figure 1). These results corroborate that direct disruption of the *mpv17* ORF results in iridophore defects.

We subsequently raised Cas9 RNP-injected mosaic crispants with iridophore loss to adulthood. While strikingly visible at early stages, we observed a gradual recovery in iridophores over time and crispants were virtually indistinguishable from wildtype controls at 3 months of age (data not shown). We suspect that iridophore recovery is possible due to the mosaic nature of our transient mutagenesis assay. To isolate germline mutants, we incrossed F0 crispant siblings and observed the resulting F1 for phenotypes. Incrosses of $mpv17^{ccB}$, $mpv17^{ccC}$ as well as trans-heterozygous crosses of adult crispants resulted in F1 embryos with iridophore loss that correlated with mutant *mpv17* genotype (Figure 4F–H). Of note, we repeatedly recovered the frameshift allele $mpv17^{c.140\_144del}$ ($mpv17^{\Delta 5}$) from founders of $mpv17^{ccC}$, revealing predominant repair preference for this particular 5bp deletions using sgRNA $mpv17^{ccC}$ (Figure 4E,E′). We raised trans-heterozygous $mpv17^{\Delta 1/\Delta 5}$ to adulthood and no longer observed any recovery from the iridophore loss. Compared to wildtype, 3 month old $mpv17^{\Delta 1/\Delta 5}$ were completely devoid of iridophores in the eye and

also displayed a nearly complete iridophore loss along the body axis. In addition to the irididophore loss trans-heterozygous mutants also failed to correctly form melanocytes in their longitudinal stripes (Figure 4L, M). Taken together, these experiments confirm that direct perturbation of the *mpv17* ORF causes iridophore defects as observed by the *roy orbison* and *transparent* lesions.

roy^{a9} and transparent^{b6} neither complement each other nor mpv17 frameshift alleles

Our sequencing analysis and the data from Krauss et al. (Krauss et al., 2013) indicate that both *roy orbison* and *transparent*^{b6} possibly carry a lesion in intron 2–3 of *mpv17*. To further corroborate genetic relationship of the different *mpv17* alleles, we performed genetic complementation analysis (Figure 4I–K). We crossed *mpv17*^{ccB} and *mpv17*^{ccC} F0 crispants to *roy*$^{a9/a9}$;*nac*$^{w2/w2}$ (*casper*) and to *tra*$^{b6/b6}$;*nac*$^{w2/w2}$. In both crosses, genotype-confirmed offspring harboring frameshift alleles arising from *mpv17*^{ccB} and *mpv17*^{ccC} presented a strong iridophore reduction in the eye, trunk, and swimbladder area, revealing non-complementation of *roy*^{a9} and *tra*^{b6} by *de novo* mutants affecting the *mpv17* ORF. We also crossed *roy*$^{a9/a9}$;*nac*$^{w2/w2}$ to *tra*$^{b6/b6}$;*nac*$^{w2/w2}$ and observed complete penetrance of the *roy orbison* and *nacre* phenotypes, resulting in embryos that are indistinguishable from *casper*. Taken together, our complementation analysis confirms that the zebrafish mutants *roy orbison* and *transparent* form a complementation group and are allelic to *mpv17*, as further confirmed by our independently derived generated frameshift alleles. In all the allele combinations, the majority of embryos failed to completely inflate their swim bladder by 5 dpf, indicating this phenotype results also as a consequence of *mpv17* perturbation. Taken together, mutant zebrafish strains of the genotypes *roy*$^{a9/a9}$;*nac*$^{w2/w2}$ or *tra*$^{b6/b6}$;*nac*$^{w2/w2}$ look virtually identical, and our genetic complementation analysis establishes that both these genotypes result in *casper* by virtue of the identical defect in *roy*^{a9} and *tra*^{b6}.

mtDNA content in roy

Given the known role of mpv17 in mtDNA maintenance, we reasoned that the zebrafish mutant might harbor a depletion of mtDNA in the skin. Higdon and Johnson showed by RNA-seq that mpv17 is highly enriched in iridophores compared to other pigment cells such as melanocytes (Higdon et al., 2013). Krauss, et al, also recently noted that zebrafish *mpv17* also localizes to the mitochondria, similar the the human and mouse protein. Furthermore, We previously noted that the kidney of the *casper* strain appears histologically normal, in contrast to the mouse mutant for *Mpv17* (Viscomi et al., 2009). To test for loss of mtDNA, we performed array CGH (comparative genomic hybridization) in which we compared the skin and the kidney of both AB fish as well as *roy* orbison mutant. After isolating DNA from these tissues in 3 AB and 3 *roy orbison* fish, we hybridized it to Nimblegen zebrafish genome arrays, which contain probes for all autosomes as well as the mitochondrial genome. By comparing the normalized signal of the skin versus kidney in each animal, we could calculate the relative amount of mtDNA in each of these tissues, and across genotypes (Supplemental Figure 2). In the AB strain, we found that the skin generally contained more mtDNA signal compared to the kidney (log2 fold-change of skin:kidney=0.733+/−0.46 SEM). In contrast, in *roy orbison,* the exact opposite was found, where the mtDNA skin:kidney ratio was −0.742+/−0.19 ($p<0.05$, AB vs. *roy orbison,* unpaired t-test). This data

are consistent with a relative decrease in mtDNA content in the skin of *roy orbison* compared to the kidney.

DISCUSSION

The zebrafish strain *casper* is homozygous for the pigment-affecting mutations of roy^{a9} and $nacre^{w2}$. Due to its due to its transparency, it is widely used as versatile background for *in vivo* imaging and transplantation experiments. For *casper* to maintain its transparency, both the nac^{w2} and roy^{a9} alleles must be maintained as homozygous. Whereas *nac* is well-known to be due to an inactivating mutation in *mitfa* resulting in loss of pigmented melanocytes (Lister et al., 1999), the nature of the *roy* mutation has remained obscure. Here, we show that the causative lesion in *roy* is due to a loss of the mitochondrial inner membrane protein *mpv17*. The same gene was recently shown to be perturbed in the spontaneous zebrafish mutant called *transparent*, named due to the obvious transparency of its skin initiated by iridophore defects (Krauss et al., 2013). Several lines of evidence presented in our study corroborate that *roy orbison* and *transparent* affect the same gene, *mpv17*, and might be a similar or even the same allele.

Our work establishes that roy^{a9}, tra^{b6}, and our new Cas9 RNP-induced *mpv17* mutants are recessive loss-of-function alleles of the same locus as shown by non-complementation. F0 mosaic Cas9-induced mutants, so-called crispants, readily recapitulate how lesions in the *mpv17* ORF cause iridiophore defects. Nonetheless, *mpv17* F0 crispants recover and appear wildtype with increasing age; this phenomenon likely reflects how wildtype or hypomorphic clones of cells replace unfit, mutant clones in genetic mosaics, posing a major caveat of somatic mutant analysis. Our readily isolated germline F1 mutants subsequently confirmed the mutant phenotype and non-complementation with roy^{a9} and tra^{b6}. These experiments underline the value of using Cas9 to generate *de novo* alleles of mutant candidate genes to perform complementation analysis and phenotype comparisons.

The most-striking finding of our investigation is the remarkably similar nature of the genetic lesion causing the roy^{a9} and tra^{b6} alleles: without featuring any exon lesions, both mutants feature mis-spliced exons 2 and 3, resulting in the identical frameshift and premature stop codon. As already Krauss et al. discovered for tra^{b6}, we find that intron 2–3 of roy^{a9} features a deletion that we also failed to properly chart; hence, roy^{a9} and tra^{b6} must harbor highly similar lesions. It is not clear whether intron 2–3 of *mpv17* could have a tendency to accumulate spontaneous mutations. An alternative explanation remains that roy^{a9} and tra^{b6} are indeed descending from the same founder mutation and represent the same strain. Regardless of their origin, our complementation analysis confirms that *roy orbison* and *transparent* both affect *mpv17*. Consequently, compound mutant strains of $tra^{b6/b6};nac^{w2/w2}$ result in virtually identical animals as $roy^{a9/a9};nac^{w2/w2}$ compound homozygotes, both establishing the *casper* phenotype by the same genetic lesions.

The molecular function of *mpv17* has remained elusive for nearly two decades. As recently reviewed by Löllgen and Weiher (Löllgen and Weiher, 2015), there is significant inter-species differences in the consequences of *mpv17* mutation. In humans, the primary defect seems to occur in the liver, with a severe loss of mtDNA and the clinical syndrome most

severe with hepatocerebral disease, often occurring in young children. In contrast, the mouse mutant, which has been extensively analyzed, was originally noted for its severe renal disease resembling focal segmental glomerulosclerosis. Interestingly, the liver in the mouse shows the expected large decrease in mtDNA content, with only 4% of the content compared to WT. In contrast, the kidney is less affected in this regard, with overall 60% of the levels seen in WT, but even within this tissue the effect is heterogeneous, with the glomerular podocytes severely affected while the renal tubules were relatively normal(Spinazzola et al., 2006). In our studies, we find that overall the skin of the *roy orbison* animals do show a decrease in mtDNA, at least judged by aCGH signal. However, one major limitation of our study is that we could not isolate specific cell types from within the skin such as the iridophores. It is likely that our results could simply reflect the fact that the iridophores are absent from the skin in *roy orbison,* and if the iridophores are especially rich in mtDNA this would be reflected in the lower mtDNA signal in array CGH. Methods to more specifically isolate and analyze iridophore mtDNA content from the zebrafish will be necessary to elucidate the precise role of mtDNA depletion in the pigment defect we see in the fish.

In contrast to humans or even mice with mutations in *mpv17*, we see no gross defects in liver, kidney or muscle in our fish, with the majority of defects confined to the skin. It is possible that under certain stressors, defects in these other tissues could become apparent. We did observe an obvious defect or delay in swim bladder inflation, which could potentially hamper proper swimming at early larval stages, with possibly detrimental consequences for survival and behavior. Nonetheless, we find that in general the *casper* strain maintains excellent health and fecundity throughout its lifespan. Early generations of *casper* did show poor survival likely caused by inbreeding, as we found that outcrossing *casper* to the wild EkkWill strain restores full health and potency of *casper.* Hence, under most laboratory conditions, the mutation in *mpv17* functionally impairs only a limited number of cell types within the zebrafish. This makes *roy orbison/transparent/mpv17* mutants, and by extension *casper* itself, an excellent model for investigating tissue-specific defects in mtDNA maintenance and in mitochondrial function.

METHODS

Zebrafish husbandry and maintenance

All zebrafish were maintained in a temperature-controlled (28.5C), light-controlled (14h on/10h off) room as per standard conditions. Embryos were raised in temperature-controlled (28.5°C) incubators in E3 medium. *AB* and *WIK* strains were obtained from the ZIRC zebrafish stock center (Eugene, OR); *TE* was a generous gift from Patrick Müller (MPI Tübingen); *roy orbison* was originally obtained from the Dowling laboratory (Harvard Medical School); $tra^{b6/b6};nac^{w2/w2}$ from the Gilmour laboratory (EMBL Heidelberg).

Positional cloning of roy orbison

Positional cloning was performed as previously described (Zhou and Zon, 2011). Briefly, adult *roy orbison* mutants were bred to homozygous WIK fish to obtain heterozygous progeny. S from this group were then incrossed, and the embryonic offspring screened at 3–4dpf to look for defects in eye iridophores. This revealed Mendelian segregation of the *roy*

orbison phenotype, with ~25% of offspring having severely reduced or absent iridophores. A total mapping panel of 1672 fish were then used for low-resolution linkage analysis, which placed the defect on *roy* on linkage group 20. We then ped medium and high resolution mapping using previously described SNP markers along chromosome 20, as shown in Figure 2. For the fine-resolution mapping between markers z13672 and z28453, custom designed PCR primers based on the Zv9 zebrafish build were used, which led to few recombinants between markers zp6 and zp10, with only 8 genes in that interval. Based on this small number of genes, we chose a candidate approach and examined expression by ISH and qRT-PCR, revealing the gene *mpv17* to be the most likely candidate in this region.

cDNA cloning of mpv17

3 *AB* adults and and 3 *roy orbison* adults were tail-clipped, and RNA isolated using Trizol and the RNEasy kits. This was followed by reverse transcription using SuperScript III with both oligo-*dT* and random hexamers. The entire *mpv17* ORF was PCR-amplified, and cloned into the TOPO/TA cloning vector. 4–5 colonies from each TOPO reaction was mini-prepped and subject to Sanger sequencing. The sequence traces were compared to the reference genome sequence.

mRNA rescue

The full-length *mpv17* cDNA from the *AB* strain was subcloned into the *pCS2+* vector. Capped mRNA was transcribed using the mMessage machine kit per manufacturer's protocol. mRNA was resuspended in water and microinjected into 1-cell *roy* embryos at 100ng/μl. Embryos were scored for rescue of eye iridophores at 4–7 dpf.

Morpholino phenocopy

An ATG translation-blocking morpholino was designed by GeneTools using the *AB* reference sequence. The morpholino was resuspended in water, and microinjected into 1-cell AB embryos at doses ranging from 0.02mM to 4mM. Embryos were scored for loss of eye iridophores at 4–7 dpf.

Array CGH

Genomic DNA was isolated from the skin and kidney of 3 *AB* and 3 *roy* adults. This DNA was hybridized to Nimblegen zebrafish DNA arrays, as previously described (Chen et al., 2013; Freeman et al., 2009). This array has both autosomes in linkage groups 1–25, as well as mitochondrial probes. After normalization for probe intensities, a log2-fold change of skin versus kidney for each individual fish was obtained. The values across each of the three fish for each genotype was averaged.

Statistics

Iridophore counts between groups were compared using unpaired t-tests with a significance level of 0.05. The array CGH data was compared by averaging of replicates and comparison by t-test for mitochondrial chromosome (chrM) DNA signal.

sgRNA synthesis and genotyping

The *mpv17* sgRNA was designed using CHOPCHOP (Labun et al., 2016; Montague et al., 2014) (http://chopchop.cbu.uib.no/index.php). sgRNA sequences are (PAM underlined):

sgRNA[$mpv17^{ccB}$]: *5′-GATGGCCAAACACCCATGGAAGG-3′*,

sgRNA[$mpv17^{ccC}$]: *5′-GGTGCGTCTCGCGTTGTGATTGG-3′*

sgRNA synthesis using oligo-based, cloning-free template generation and *in vitro* transcription (Bassett et al., 2013; Burger et al., 2016). Primers for oligo based sgRNA synthesis were: sgRNA $T7^{fwd}$: *5′- GAAATTAATACGACTCACTATA-N20-GTTTTAGAGCTAGAAATAGC-3′*, where N20 indicates the sgRNA target sequence without PAM and the invariant $sgRNA^{rev}$: *5′-AAAAGCACCGACTCGGTGCCACTTTTTCAAGTTGATAACGGACTAGCCTTATTTTAACTTGCTATTTCTAGCTCTAAAAC-3′* (PAGE-purified, Sigma Aldrich). Primer extension was performed using Phusion polymerase (Thermo Scientific), followed by column purification and *in vitro* transcription using T7 RNA polymerase (Roche). sgRNAs were assembled with Cas9-EGFP into ribonucleopeotein complexes (RNP) solubilized with 300 mM KCL as described and were injected into 1-cell stage embryos of the *TE* wildtype strain. F1 animals were genotyped and alleles recovered by amplifying the locus using PCR primers $ccB^{forward}$*: 5′-TAACCGTTTGTCATAATGTGGC-3′*, $ccB^{reverse}$ *5′-CTAAACAAACTGCTGCTTAGGGAG-3,* $ccC^{forward}$ *5′-AATAGGGAGTGAATGGGG-3′ and* $ccC^{reverse}$ *5′-GTGGCCAGCAAAATGTAAA-3′*; resulting PCR products were sub-cloned into pJet and sequenced from DNA column-free isolated off colony PCR of individual clones, as established before. The panel plots describing the *mpv17* alleles were generated using the CrispRVariantsLite software (Lindsay et al., 2016) (http://imlspenticton.uzh.ch:3838/CrispRVariantsLite/) from clonal Sanger sequencing data of PCR clones from individual embryos.

Crispant and complementation phenotype assessment

Injected clutches were sorted for Cas9-EGFP-positive embryos 3 hours post-injection to quality-control injections and mortality was assessed at 24 hpf. Phenotypes were assessed at 3 dpf by stereomicroscopy. Statistical analysis and graphical representation were performed with GraphPad Prism 7. Embryos for imaging were raised in E3 and treated with 3% MS-222 (pH = 7) during screening and imaging. Image acquisition of $mpv17^{ccB}$ crispants and control embryos was performed with a Leica M205 FA stereomicroscope equipped with a 1x magnification lens at 100x magnification. Iridophores were visualized by illuminating embryos from above with a swan neck light source attached to the base of the stereomicroscope. Images were processed with ImageJ 1.51h and Adobe Photoshop CS6.

Supplementary Material

Refer to Web version on PubMed Central for supplementary material.

Acknowledgments

We thank the lab of Dr. Nadia Mercader for supplying the Mosimann lab with additional *casper* adults, and the lab of Dr. Darren Gilmour for *transparent* mutants. We thank Sibylle Burger for technical assistance, Eliane Escher for sequencing services, Kara Dannenhauer and Dr. Stephan Neuhauss for zebrafish husbandry support.

This work was supported by the Canton of Zürich and the Foundation for Research in Science and the Humanities at the University of Zürich, a Swiss National Science Foundation (SNSF) professorship [PP00P3_139093] and a Marie Curie Career Integration Grant from the European Commission [CIG PCIG14-GA-2013-631984] to C.M.; an UZH URPP "Translational Cancer Research" grant to A.B.; a UZH CanDoc Forschungskredit to G.D. The NIH Director's New Innovator Award (DP2CA186572), Mentored Clinical Scientist Research Career Development Award (K08AR055368), The Melanoma Research Alliance Young Investigator Award, The Alan and Sandra Gerry Metastasis Research Initiative at the Memorial Sloan Kettering Cancer Center, The Harry J. Lloyd Foundation and Consano (R.M.W.).

References

Bassett AR, Tibbit C, Ponting CP, Liu JL. Highly efficient targeted mutagenesis of Drosophila with the CRISPR/Cas9 system. Cell Rep. 2013; 4:220–228. DOI: 10.1016/j.celrep.2013.06.020 [PubMed: 23827738]

Burger A, Lindsay H, Felker A, Hess C, Anders C, Chiavacci E, Zaugg J, Weber LM, Catena R, Jinek M, Robinson MD, Mosimann C. Maximizing mutagenesis with solubilized CRISPR-Cas9 ribonucleoprotein complexes. Development. 2016; 143:2025–2037. DOI: 10.1242/dev.134809 [PubMed: 27130213]

Chen EY, Dobrinski KP, Brown KH, Clagg R, Edelman E, Ignatius MS, Chen JYH, Brockmann J, Nielsen GP, Ramaswamy S, Keller C, Lee C, Langenau DM. Cross-species array comparative genomic hybridization identifies novel oncogenic events in zebrafish and human embryonal rhabdomyosarcoma. PLoS Genet. 2013; 9:e1003727.doi: 10.1371/journal.pgen.1003727 [PubMed: 24009521]

Freeman JL, Ceol C, Feng H, Langenau DM, Belair C, Stern HM, Song A, Paw BH, Look AT, Zhou Y, Zon LI, Lee C. Construction and application of a zebrafish array comparative genomic hybridization platform. Genes Chromosomes Cancer. 2009; 48:155–170. DOI: 10.1002/gcc.20623 [PubMed: 18973135]

Higdon CW, Mitra RD, Johnson SL. Gene expression analysis of zebrafish melanocytes, iridophores, and retinal pigmented epithelium reveals indicators of biological function and developmental origin. PLoS ONE. 2013; 8:e67801.doi: 10.1371/journal.pone.0067801 [PubMed: 23874447]

Krauss J, Astrinidis P, Frohnhöfer HG, Walderich B, Nüsslein-Volhard C. transparent, a gene affecting stripe formation in Zebrafish, encodes the mitochondrial protein Mpv17 that is required for iridophore survival. Biol Open. 2013; 2:703–710. DOI: 10.1242/bio.20135132 [PubMed: 23862018]

Labun K, Montague TG, Gagnon JA, Thyme SB, Valen E. CHOPCHOP v2: a web tool for the next generation of CRISPR genome engineering. Nucleic Acids Res. 2016; 44:W272–6. DOI: 10.1093/nar/gkw398 [PubMed: 27185894]

Lindsay H, Burger A, Biyong B, Felker A, Hess C, Zaugg J, Chiavacci E, Anders C, Jinek M, Mosimann C, Robinson MD. CrispRVariants charts the mutation spectrum of genome engineering experiments. Nat Biotechnol. 2016; 34:701–702. DOI: 10.1038/nbt.3628 [PubMed: 27404876]

Lister JA, Robertson CP, Lepage T, Johnson SL, Raible DW. nacre encodes a zebrafish microphthalmia-related protein that regulates neural-crest-derived pigment cell fate. Development. 1999; 126:3757–3767. [PubMed: 10433906]

Löllgen S, Weiher H. The role of the Mpv17 protein mutations of which cause mitochondrial DNA depletion syndrome (MDDS): lessons from homologs in different species. Biol Chem. 2015; 396:13–25. DOI: 10.1515/hsz-2014-0198 [PubMed: 25205723]

Lopes SS, Yang X, Müller J, Carney TJ, McAdow AR, Rauch GJ, Jacoby AS, Hurst LD, Delfino-Machín M, Haffter P, Geisler R, Johnson SL, Ward A, Kelsh RN. Leukocyte tyrosine kinase functions in pigment cell development. PLoS Genet. 2008; 4:e1000026.doi: 10.1371/journal.pgen.1000026 [PubMed: 18369445]

McGowan KA, Barsh GS. Evolution: How the zebrafish got its stripes. elife. 2016; :5.doi: 10.7554/eLife.14239

Montague TG, Cruz JM, Gagnon JA, Church GM, Valen E. CHOPCHOP: a CRISPR/Cas9 and TALEN web tool for genome editing. Nucleic Acids Res. 2014; 42:W401–7. DOI: 10.1093/nar/gku410 [PubMed: 24861617]

Parichy DM, Mellgren EM, Rawls JF, Lopes SS, Kelsh RN, Johnson SL. Mutational analysis of endothelin receptor b1 (rose) during neural crest and pigment pattern development in the zebrafish Danio rerio. Dev Biol. 2000; 227:294–306. DOI: 10.1006/dbio.2000.9899 [PubMed: 11071756]

Parichy DM, Spiewak JE. Origins of adult pigmentation: diversity in pigment stem cell lineages and implications for pattern evolution. Pigment Cell Melanoma Res. 2015; 28:31–50. DOI: 10.1111/pcmr.12332 [PubMed: 25421288]

Rawls JF, Mellgren EM, Johnson SL. How the zebrafish gets its stripes. Dev Biol. 2001; 240:301–314. DOI: 10.1006/dbio.2001.0418 [PubMed: 11784065]

Ren JQ, McCarthy WR, Zhang H, Adolph AR, Li L. Behavioral visual responses of wild-type and hypopigmented zebrafish. Vision Res. 2002; 42:293–299. [PubMed: 11809482]

Spinazzola A, Viscomi C, Fernandez-Vizarra E, Carrara F, D'Adamo P, Calvo S, Marsano RM, Donnini C, Weiher H, Strisciuglio P, Parini R, Sarzi E, Chan A, DiMauro S, Rötig A, Gasparini P, Ferrero I, Mootha VK, Tiranti V, Zeviani M. MPV17 encodes an inner mitochondrial membrane protein and is mutated in infantile hepatic mitochondrial DNA depletion. Nat Genet. 2006; 38:570–575. DOI: 10.1038/ng1765 [PubMed: 16582910]

Viscomi C, Spinazzola A, Maggioni M, Fernandez-Vizarra E, Massa V, Pagano C, Vettor R, Mora M, Zeviani M. Early-onset liver mtDNA depletion and late-onset proteinuric nephropathy in Mpv17 knockout mice. Hum Mol Genet. 2009; 18:12–26. DOI: 10.1093/hmg/ddn309 [PubMed: 18818194]

White RM, Sessa A, Burke C, Bowman T, LeBlanc J, Ceol C, Bourque C, Dovey M, Goessling W, Burns CE, Zon LI. Transparent adult zebrafish as a tool for in vivo transplantation analysis. Cell Stem Cell. 2008; 2:183–189. DOI: 10.1016/j.stem.2007.11.002 [PubMed: 18371439]

Zhou Y, Zon LI. The zon laboratory guide to positional cloning in zebrafish. Methods Cell Biol. 2011; 104:287–309. DOI: 10.1016/B978-0-12-374814-0.00016-1 [PubMed: 21924169]

Highlights

- -the casper strain of zebrafish is widely used for imaging of adult fish
- -casper is a compound mutant composed of both nacre (mitfa) and roy orbison (an unknown gene)
- -here the authors identify a mutation in the gene mpv17 as the underlying cause of the roy orbison phenotype
- -this leads to a severe defect in iridophore development, and is identical to the recently described transparent mutant

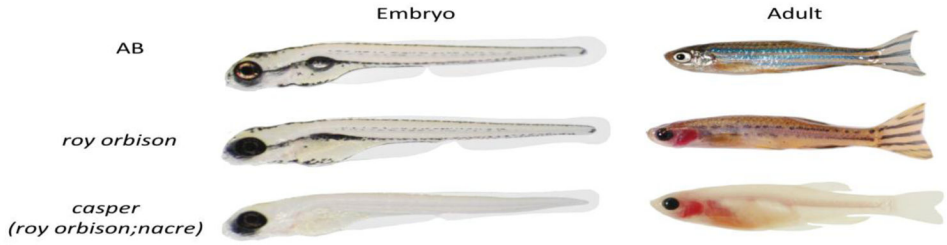

Figure 1.

The *roy* orbison mutant phenotype, one of the two strains found in the transparent casper strain. During embryogenesis, *roy* lacks nearly all reflective iridophores, but melanophore development is relatively normal. In contrast, as adults, *roy* has a severe defect in both iridophores and melanophores. casper is largely similar to *roy* except that it also has a mutation in mitfa, leading to complete loss of all pigmented melanocytes.

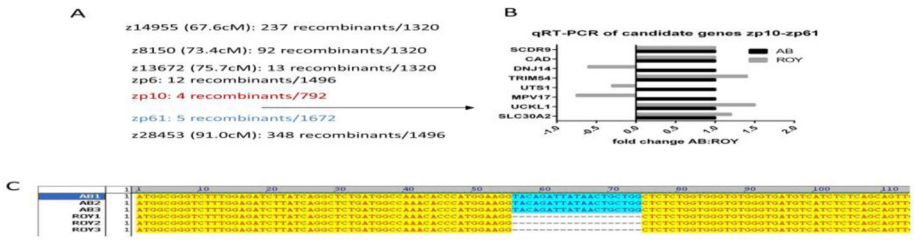

Figure 2.

Genetic linkage map of the roy orbison mutant. (A) Chromosome 20 map with SNP markers showing the number of recombinants at each location. The *roy* mutant was located between markers zp10 and zp61. (B) Quantitative RT-PCR for all 8 genes located in the *roy* interval, to identify likely candidates showing decreased RNA likely due to nonsense mediated decay. Only three genes, DNJ14, UTS1 and MPV17, showed a decrease in the mRNA. Because MPV17 is expressed in the neural crest, this was the most likely candidate. (C) cDNA sequencing of the MPV17 locus was done in 3 wild-type AB and 3 mutant *roy* orbison fish. Clones from each animal were sequenced by Sanger sequencing, and in all 3 mutant fish showed a 19bp deletion between exons 2 and 3, leading to an early stop codon.

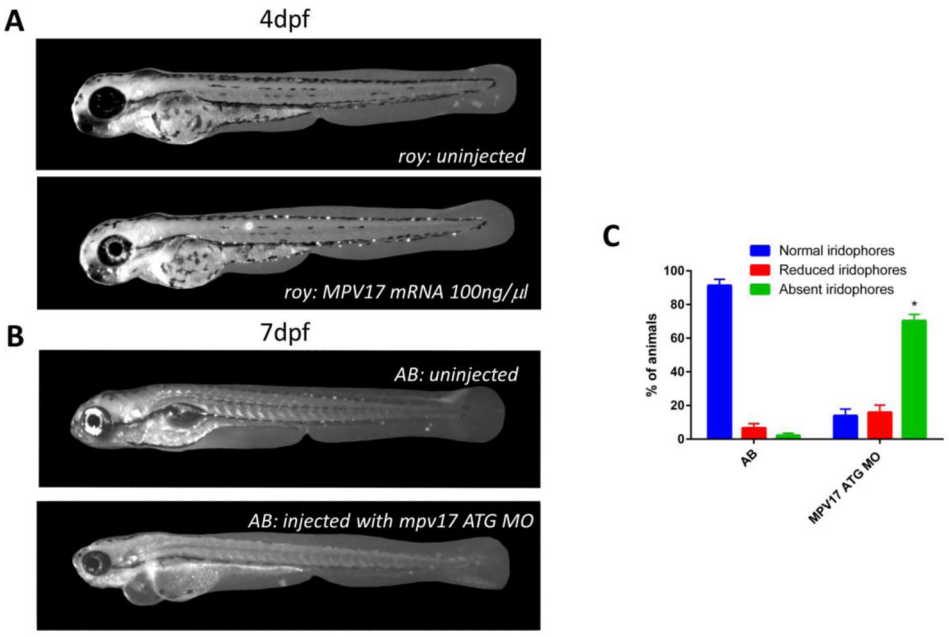

Figure 3.

(A) Injection of full-length mpv17 mRNA leads to rescue of the *roy* orbison mutant phenotype, as demonstrated by the appearance of iridophores both in the eye and throughout the body of the fish (*roy* n=0/20 fish with eye iridophores, *roy*+mRNA injection, n=14/20 fish with eye iridophores). (B) ATG morpholino knockdown of MPV17 in the AB fish leads to a strong phenocopy of the *roy* phenotype, with loss of eye and body iridophores (AB =71/79 fish with eye iridophores, AB+morpholino injection, n=8/67 fish with eye iridophores). (C) Quantification of eye iridophores after morpholino injection to mpv17 shows a significant increase in # of fish with absent iridophores (*, $p<0.05$, paired t-test)

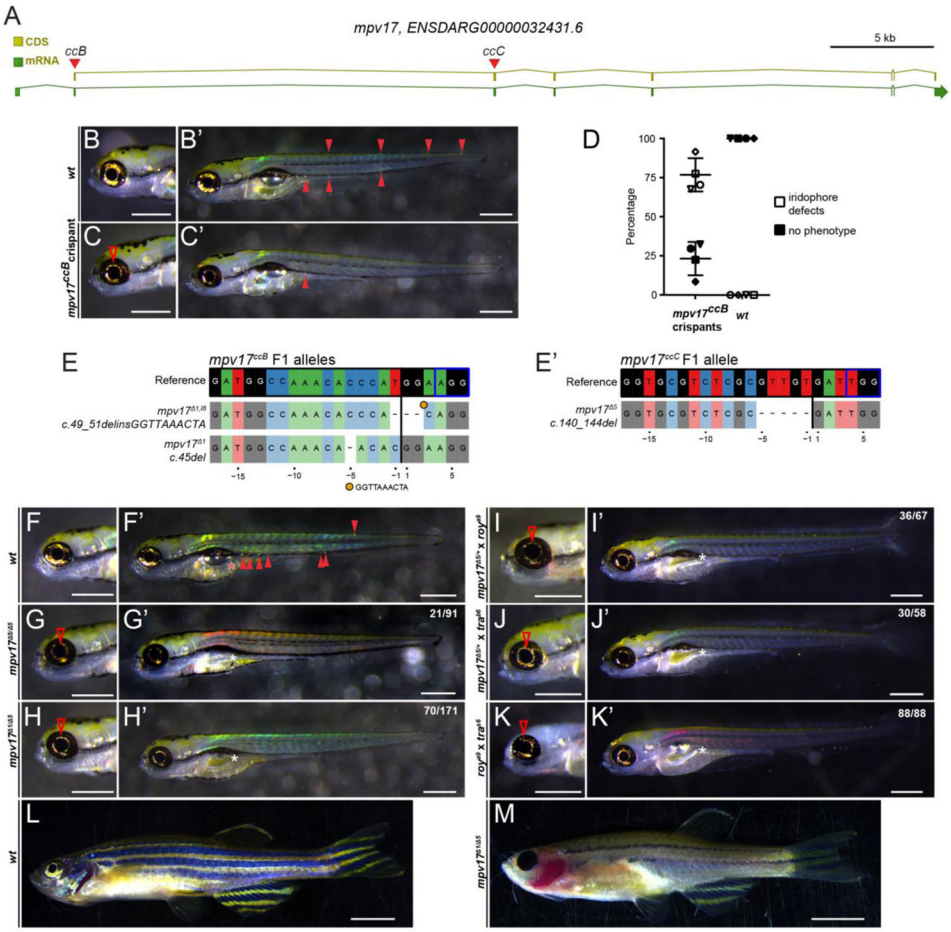

Figure 4.

A) Schematic of the zebrafish mpv17 locus, with coding sequence (CDS) and total mRNA-coding region including introns, red triangles depict sgRNA locations ccB and ccC in coding exons. (B,B′) Brightfield imaging of 5 dpf zebrafish embryos to visualize iridophores, anterior to the left; scale bars represent 500 μm. Wildtype (wt) control showing prominent iridophores surrounding the eye lens and as individual cells along the body (solid arrowheads). (C,C′) Representative Cas9 RNP-injected, somatic-mutant embryo (crispant) where the ORF of mpv17 was targeted with sgRNA ccB in coding exon 1; note diminished iridophores in eye (red arrowhead) and severe reduction of body iridophores. (D) Phenotype distribution in mpv17ccB crispants versus wt controls. (E,E′) Mutant mp 17 alleles isolated in the F1 generation injected with sgRNA ccB (left) and ccC (right) and recovered in complementation analysis; genomic reference sequence depicted on top, black vertical bar indicates Cas9 cleavage site, blue box depicts PAM. (F, F′) Wildtype (wt) forms iridophores in eye and along the body (red arrowhead) and properly inflates the swimbladder (red asterisks). (G–H) Homozygous mp 17Δ5 and trans-heterozygous mp 17Δ1/Δ5 embryos show severe reduction of iridophores. (I,J) The same phenotype occurs in embryos trans-heterozygous for mp 17Δ5 and roy^{a9} (I, I′) or mp 17$^{\Delta 5}$ and tra^{b6} (J,J′) as confirmed by genotyping for mp 17Δ5 (n=4). (K,K′) Trans-heterozygous embryos for roya9 and tra^{b6} also show severe iridophore reduction, establishing non-complementation between roy^{a9} and

tra^{b6} as mutant alleles of mpv17. (L) 3 month old wildtype with iridophores in the eye and along the body and melanocytes form normally into longitudinal stripes. (M) Trans-heterozygous mp 17Δ1/Δ5 fish completely lack eye iridophores and most iridophores along the body axis. Melanocytes in the stripes are heavily reduced. Scale bars represent 5 mm. White asterisks in whole embryo views mark failed inflation of the swimbladder in all observed mpv17 mutant combinations.